JGR Biogeosciences

RESEARCH ARTICLE
10.1029/2023JG007991

Key Points:

- Storm surge and high tides are leading to marsh loss and mangrove establishment
- Mangrove expansion is increasing CO_2 sequestration
- Mangrove colonization in marshes is driving a net cooling forcing

Supporting Information:

Supporting Information may be found in the online version of this article.

Correspondence to:

G. Starr,
gstarr@ua.edu

Citation:

Yannick, D., Oberbauer, S., Staudhammer, C., Cherry, J., & Starr, G. (2024). Carbon dynamics of a coastal wetland transitioning to mangrove forest. *Journal of Geophysical Research: Biogeosciences*, *129*, e2023JG007991. https://doi.org/10.1029/2023JG007991

Received 26 DEC 2023
Accepted 7 MAR 2024

Author Contributions:

Conceptualization: D. Yannick, S. Oberbauer, C. Staudhammer, J. Cherry, G. Starr
Data curation: D. Yannick, C. Staudhammer, G. Starr
Formal analysis: D. Yannick, C. Staudhammer
Funding acquisition: S. Oberbauer, C. Staudhammer, G. Starr
Investigation: D. Yannick, S. Oberbauer, C. Staudhammer, G. Starr
Methodology: D. Yannick, S. Oberbauer, C. Staudhammer, G. Starr
Project administration: S. Oberbauer, C. Staudhammer, G. Starr
Resources: S. Oberbauer, C. Staudhammer, J. Cherry, G. Starr
Supervision: S. Oberbauer, C. Staudhammer, J. Cherry, G. Starr
Validation: D. Yannick, J. Cherry
Writing – original draft: D. Yannick
Writing – review & editing: D. Yannick, S. Oberbauer, C. Staudhammer, J. Cherry, G. Starr

Carbon Dynamics of a Coastal Wetland Transitioning to Mangrove Forest

D. Yannick[1], S. Oberbauer[2], C. Staudhammer[1], J. Cherry[1,3], and G. Starr[1]

[1]Department of Biological Sciences, University of Alabama, Tuscaloosa, AL, USA, [2]Institute of Environment and Department of Biological Sciences, Florida International University, Miami, FL, USA, [3]New College, University of Alabama, Tuscaloosa, AL, USA

Abstract Coastal wetlands play a vital role in the global carbon cycle and are under pressure from multiple anthropogenic influences. Altered hydrology and land use change increase susceptibility of wetlands to sea-level rise, saltwater intrusion, tidal flood events, and storm surges. Flooding from perigean spring tides and storm surges rapidly inundates coastal wetlands with saline waters, quickly surpassing vegetation tolerances, leading to shifts in soil microbial respiration, peat collapse, and plant mortality, followed by establishment of salt-tolerant vegetation. The Southeast Saline Everglades (SESE) is facing many of these pressures, making it a model system to examine the impacts of ecosystem state transitions and their carbon dynamics. Saltwater flooding from Hurricane Irma (2017) initiated a transitional state, where less salt-tolerant vegetation (e.g., *Cladium jamaicense*) is declining, allowing halophytic species such as *Rhizophora mangle* to colonize, altering the ecosystem's biogeochemistry. We utilized eddy covariance techniques in the SESE to measure ecosystem fluxes of CO_2 and CH_4 in an area that is transitioning to an alternative state. The landward expansion of mangroves is increasing leaf area, leading to greater physiological activity and higher biomass. Our site was presented initially as a small C source (47.0 g C m^{-2}) in 2020, and by 2022 was a sink (−84.24 g C m^{-2}), with annual greenhouse carbon balance ranging from −0.04 to 0.18. Net radiative forcing ranged from 2.04 to 2.27 W m^{-2} d^{-1}. As the mangrove landward margin expands, this may lead the area to become a greater carbon sink and a potential offset to increasing atmospheric CO_2 concentrations.

Plain Language Summary Hurricane-caused storm surge and king tides have led to increasing amounts of saltwater being deposited inland. Inland flooding causes increased salinity in freshwater marshes, leading to mortality in marsh plants that are less tolerant to salt. At the same time, inland flooding pushes mangrove propagules inland and allows them to rapidly establish. Mangroves have high saline tolerance and accumulate salt in their leaves. Mangroves can further increase salt concentrations when they drop their leaves, which may increase the mortality of existing marsh vegetation and enhance the expansion of mangroves. As these mangrove trees increase in number and size, they can capture more carbon dioxide from the atmosphere compared to the previous vegetation. If this trend continues these new mangrove-dominated systems may aid in slowing or mitigating atmospheric increases in CO_2.

1. Introduction

Wetlands are highly productive ecosystems that have a vital biogeochemical role in mitigating climate change as carbon (C) sinks (Mitsch et al., 2013; Reddy & DeLaune, 2008). Coastal wetlands, however, are susceptible to impacts from changing disturbance regimes caused by climate change (Day et al., 2008). These ecosystems exist between the freshwater and marine ecotone, and are subject to sea level rise, storm surge from tropical cyclones, and significant tidal events such as perigean spring tides (A.K.A. king tides), exposing them to saltwater flooding and accelerated saltwater intrusion (Tully et al., 2019). Amid the challenges posed by these disturbance regimes, the inherent resiliency of coastal wetlands becomes ever more crucial. Human alterations in hydrology, such as the creation of levees, dredging, and canal construction, have compounded the stress on many of these wetlands (Richardson, 2010). These compounded stressors can diminish the resilience of coastal areas, in terms of their ability to recover from disturbance events, which could cause saltwater to be driven further landward, increasing the likelihood of an ecosystem state change (Herbert et al., 2015).

Saltwater flooding caused by storm surges and perigean spring tides are pulse disturbances that deliver a rapid increase of salinity to coastal wetlands. While this has biogeochemical implications, saltwater flooding also has biophysical effects (Neubauer, 2013). Less salt-tolerant vegetation becomes stressed leading to mortality

and soil microbial respiration changes which can drive carbon release through peat collapse (Steinmuller et al., 2019; Wilson et al., 2018). Saltwater flooding also provides a mechanism to deliver mangrove propagules inland beyond their current range (Jiang et al., 2014), which can initiate a transition to a new ecosystem (DeBusk et al., 2015; Sternberg et al., 2007). The associated changes in vegetation structure can cause a homogenization of the landscape and a change in ecosystem services (Costanza et al., 1997; Herbert et al., 2015). As saltwater flooding events are expected to increase with more frequent hurricanes and perigean spring tides, it is important to build a better understanding of their impact on coastal wetlands.

While extensive research has been conducted on the climate-driven phenomenon of mangrove poleward expansion and encroachment into salt marshes (Alongi, 2020; Osland, Day, et al., 2017), a gap exists in our understanding of the landward expansion of this species. In South Florida, freshwater coastal marshes are in a precarious position, subjected to various stressors that have set the stage for state changes. The impacts of hydrologic alterations and the persistent threat of saltwater intrusion have been documented as far back as the 1950s (Egler, 1952), predicting a gradual shift that has brought this ecosystem to the brink of transitioning into a new state.

In 2017 Hurricane Irma made landfall in Florida, causing substantial saltwater flooding in coastal wetlands of the Southeast Saline Everglades (SESE). This coincided with red mangrove (*Rhizophora mangle*) seasonal propagule dispersal and establishment in the area. Increased salinity has also contributed to the die-off of sawgrass (*Cladium jamaicense*). This transition from sawgrass to mangrove has been continually reinforced through flooding events from perigean spring tides and mangrove-driven physiological feedback (Ball, 1988). Vegetation changes in these ecosystems have led to altered C dynamics and uncertainty in the future capacity to recapture lost C (Dang et al., 2019). While the landward movement of *R. mangle* into formerly *C. jamaicense* dominated marshes has been previously documented (Ross et al., 2000), there is a limited understanding of the biogeochemical changes that are occurring in these coastal wetlands during the transition to a mangrove forest. This study addresses this knowledge gap by answering the following research questions: (a) How will carbon dynamics (net ecosystem exchange of CO_2 [NEE], gross ecosystem exchange of CO_2 [GEE], ecosystem respiration [R_{eco}], and methane [CH_4] efflux change in a coastal ecosystem during the transitional state from a marsh to mangrove forest? and (b) How will changes in carbon dynamics affect the ecosystem's greenhouse carbon balance (GCB) and radiative forcing potential? To explore our proposed questions, we collected carbon flux and micrometeorological data within the SESE over 3 years using eddy covariance (EC) techniques.

2. Methods

2.1. Study Site

Our study was conducted in the Florida Coastal Everglades, which are subtropical wetlands with distinct wet and dry seasons. Annual precipitation is ~1,300 mm, with 60% of rainfall occurring during the wet season months (May to November) (Davis & Ogden, 1994; National Climatic Data Center, 2023). Wet season mean daily temperatures range from 30 to 35°C, whereas dry season temperatures range from 12 to 24°C. The study site is located ~3.5 km from the ocean in a region initially described as being a part of "Belt 3" of the SESE, dominated by sawgrass (Egler, 1952). This portion of the Everglades is subject to marine influence due to impoundment from the Atlantic Coastal Ridge to the north and proximity to Florida and Biscayne Bays. Currently, the site's vegetation is mixed sawgrass, black rush (*Juncus roemerianus*), and red mangrove. Saltwater flooding from Hurricane Irma initiated sawgrass to die off and mangrove propagules to establish, further expanding its dominance across the site. Soils are predominately marl (fluvaquents of Perrine or Pennsuco series), with composition driven by the metabolic activities of benthic periphyton and senesced plant material (Ross et al., 2022; USDA-NRCS, 1996). Marl soils of the SESE are very low in organic matter and total soil carbon in comparison to peat soils (Steinmuller et al., 2021). The site is tidally influenced during the wet season with observed salinity ranging from 3 to 20 psu during the study period. Water depth is near the soil surface during dry periods, with soils remaining saturated and ponding in depressional areas. Wet season water depth typically ranges from 20 to 40 cm. The study site, herein referred to by the Ameriflux designation, US-EVM, was established in February 2020, and data were collected through 31 May 2023.

2.2. Eddy Covariance Measurements

Flux data collection commenced on 1 May 2020. Open-path infrared gas analyzers (IRGAs) were used to measure ecosystem fluxes of CH_4 (mol m^{-3}; LI-7700 Li-COR Inc., Lincoln, NE), CO_2 and H_2O (mg mol^{-1}; LI-7500 Li-COR Inc., Lincoln, NE), and were paired with a sonic anemometer (CSAT3B, Campbell Scientific Inc., Logan, UT) that measured sonic temperature (T_{sonic}; K) and 3-dimensional wind speed at 10 z (u, v, and w, respectively; m s^{-1}). The tower height was approximately 4 m above ground level with paired sensors placed ∼0.20 m apart. The EC data were collected on the LI-COR SmartFlux data acquisition system (LI-COR Inc., Lincoln, NE) and stored on an industrial USB drive. IRGAs were calibrated monthly using a trace gas standard for CO_2 and CH_4 in air (+1.0%), dry N_2 gas, and a portable dewpoint generator (LI-610, LI-COR Inc.).

2.3. Meteorological Variables

Commencing 1 February 2020, meteorological data were collected half-hourly on a separate data logger (CR3000, Campbell Scientific Inc), including T_{air} (°C) and relative humidity (Rh; %) (HMP60C, Vaisala, Helsinki, Finland) mounted within an aspirated shield (43502, R.M. Young Co., Traverse City, MI), and barometric pressure (P; Pa) (PTB110, Vaisala). The T_{air}/Rh sensors were installed at the same height above ground as the IRGA and CSAT. Other meteorological data were collected as 30-min averages through a multiplexer (AM16/32A Campbell Scientific Inc.) with another datalogger (CR3000 Campbell Scientific Inc.). This included photosynthetic photon flux density (PPFD; μmol m^{-2} s^{-1}) (PAR Lite, Kipp and Zonen Inc., Delft, Netherlands), incident solar radiation (Rs; W m^{-2}) (LI-200SZ, LI-COR Inc.), and net radiation (Rn; W m^{-2}) (NR01, Hukseflux). Precipitation was measured with a tipping bucket rain gauge (mm) (TE525, Texas Electronics Inc., Dallas, TX). Soil temperature (T_{soil}; °C) was measured at 5, 10, and 20 cm depths using insulated thermocouples (Type-T, Omega Engineering Inc., Stamford, CT). Water temperature (T_{water}; °C) was measured using insulated thermocouples (Type-T, Omega Engineering Inc.) located at a fixed height 2 cm below the water surface. Water level (WL; m) was recorded every half-hour with a water level logger (HOBO U20-001-01, Onset, Bourne, MA).

2.4. Fluxes

Flux data for this study were processed with EddyPro 7.0.9, using corrections for density fluctuations and high-frequency spectral loss (Fratini & Mauder, 2014). Quality assurance was maintained by examining plausibility tests for CO_2, represented as NEE values (i.e., $|NEE| \leq 5$ μmol m^{-2} s^{-1}), stationarity criteria, and integral turbulent statistics (Foken & Leclerc, 2004; Foken & Wichura, 1996).

Raw CH_4 EC data were processed over 30-min time intervals with LI-7700 diagnostics turned off, which filter out high-frequency fluxes that could represent valid underlying variation in this system (Yu et al., 2022). Processing options and filtering followed the conventions established in Staudhammer et al. (2022). Fluxes based on mass density (ρCH_4) measurements by the LI-7700 were calculated according to McDermitt et al. (2011; Equation 1).

$$F_{CH_4} = A\overline{\left(w'\rho'_{CH_4}\right)} + B\mu\frac{\overline{\rho_{CH4}}}{p_a}\overline{w'\rho'H_2O} + C\frac{(1+\mu\sigma)\overline{\rho_{CH4}}}{\overline{T}}\overline{w'Ta'} \quad (1)$$

Where: A, B, and C are dimensionless multipliers for spectroscopic corrections, μ is the molar mass ratio of dry air to water vapor, ρ_a is the average mass density of dry air, σ is the mass density ratio of water vapor to dry air, ρ_{H_2O} is the water vapor mass density, and T_a is air temperature (°C). Overbars denote time averages over the measurement intervals. Primes denote the turbulent fluctuations in the variable.

Flux measurements for CO_2 were filtered when systematic errors were indicated, such as: (a) evidence of rainfall, condensation, or bird fouling in the sampling path of the IRGA or sonic anemometer, (b) incomplete half-hour data sets during system calibration or maintenance, (c) poor coupling of the canopy with the external atmospheric conditions, as defined by the friction velocity, U*, using a threshold of 0.15 m s^{-1} (Clark et al., 1999; Goulden et al., 1996), and (d) excessive variation from the half-hourly mean based on an analysis of standard deviations for u, v, and w wind and CO_2 statistics, (e) low signal strength (RSSI < 10%), (f) and when outside a plausibility limit of −6 to 6 μmol m^{-2} s^{-1}. The plausible range was evaluated annually with light response curves as mangroves proliferated and matured.

Measurements of CH_4 fluxes were filtered when signal strength was low (RSSI < 10%), during rainfall events (rainfall > 0 mm), and when outside of a plausible range of −4 to 4 μmol m^{-2} s^{-1}, which allowed for ∼70% collected half-hourly F_{CH_4} data to be included in subsequent analyses.

2.5. Gap-Filling

Missing half-hourly CO_2 fluxes, represented as NEE, were gap-filled using separate functions for day and night. When PPFD was >10 μmol m^{-2} s^{-1}, NEE data were gap-filled using a Michaelis-Menton approach (NEE_{day}; Equation 2), and when PPFD was ≤10 μmol m^{-2} s^{-1}, NEE data were gap-filled using an Arrhenius approach (NEE_{night}; Equation 3):

$$NEE_{day} = R_{eco} - \frac{\alpha\phi P_{max}}{\alpha\phi + P_{max}} \quad (2)$$

Where: α is the apparent quantum efficiency, Φ is PPFD, R_{eco} is ecosystem respiration (μmol CO_2 m^{-2} s^{-1}), and P_{max} is the maximum ecosystem CO_2 uptake rate (μmol CO_2 m^{-2} s^{-1}).

$$NEE_{night} = R_{eco} = R_0\, e^{bT\mathrm{air}} \quad (3)$$

Where: R_0 is the base respiration rate when air temperature is 0°C, T_{air} is air temperature (°C), and b is an empirical coefficient. In Equation 2, R_{eco} is an estimated model parameter, whereas R_{eco} measurements are the dependent variable in Equation 3. Following gap filling, GEE was calculated from half-hourly NEE and R_{eco} (Equation 4).

$$GEE = NEE - R_{eco} \quad (4)$$

To fill gaps in F_{CH4}, we utilized Random Forest (RF) algorithms following the methodology proposed by Staudhammer et al. (2022). The package randomForest (Liaw & Wiener, 2002) was used to create 500 trees by year, considering 4 variables at each split point, using 80% of the data for model training and remaining 20% for testing. Variables included as predictors included other fluxes and the suite of micrometeorological variables, but excluded variables which were highly correlated with others (e.g., net radiation): NEE, GEE, H, LE, R_{eco}, PAR, T_{air}, WL, WS, and WD. Since WD is a circular measure, we used the sine and cosine of WD as inputs to statistical models. Based on previous studies of F_{CH4}, we also included the half-day average in water level (WL_12 hr_avg), as well as the lagged 2-day average value (WL_2-day_avg) (Yu et al., 2022).

When gaps consisted of eight consecutive half-hours or less, we utilized annual "unrestricted" RF models, which accounted for synoptic patterns in F_{CH4} by including rolling intervals of 2-day, 8-day, and 32-day flux averages, as well as the suite of micrometeorological variables (NEE, GEE, H, LE, R_{eco}, PPFD, T_{air}, WL, WS, and WD). Large gaps (greater than 4 hr) were gap-filled with "restricted" models, which excluded the F_{CH4} -based predictors. First, annual training data was passed through RandomForest function to fit the unrestricted model. Then, utilizing the predict function, test data were used to generate predictions and calculate root mean squared error and mean absolute error. Then, the process was repeated using the "restricted" RF model (Table S1 in Supporting Information S1).

2.6. Carbon Budgets, Greenhouse Carbon Balance, and Radiative Forcing Potential

To calculate annual C budgets, the GCB, and net radiative forcing potential (RF), data were gap-filled for the period 1 January 2020–31 May 2023. While meteorological data were available at the site starting in February 2020, January 2020 data were obtained using observations from nearby Ameriflux sites within the Everglades (US-Elm and US-Esm).

We calculated GCB as the ratio of daily flux of CH_4 versus CO_2, and compared it to the global warming potential (GWP) of methane following Whiting and Chanton (2001). The GWP of CH_4 for 20 and 100 years is respectively 86 and 34 (Huang et al., 2013), yielding a greenhouse carbon compensation point (1/GWP) of 0.012 and 0.0029 for 20 years 100 years, respectively. GCB ratios above each compensation point indicate that CH_4 emissions are

not offset by the productivity of the ecosystem, within either 20 or 100 years. Negative ratios indicate a "cooling" forcing potential.

To calculate RF (W m^{-2}) of measured fluxes CH_4 and CO_2, we followed a simplified method of Helbig et al. (2017) and Myhre et al. (1998);

$$RF_{CO_2} = \alpha * \ln\left(\frac{\Delta C}{C_0}\right) \quad (5)$$

$$RF_{CH_4} = \alpha * \Delta C \quad (6)$$

Where α is 5.35 for CO_2 and 0.48 for CH_4, ΔC is daily change in gas concentration (CO_2 ppm, CH_4 ppb), and C_0 is the preindustrial atmospheric CO_2 concentration (280 ppm).

Generally, the wet season is defined as May through October, with the dry season occurring from November through April. However, based on the findings of Yu et al. (2022), we used a cumulative anomaly approach to define the onset and demise of wet and dry seasons. Following Noska and Misra (2016), inflection points in patterns of precipitation versus annual daily averages were identified:

$$P'_n(k) = \sum_{m=1}^{k}\left[P_n(m) - \bar{\bar{P}}\right] \quad (7)$$

Where $P_n(m)$ is the average daily rainfall for in a given year n. $\bar{\bar{P}}$ is the overall mean daily rainfall for all observations.

2.7. Statistical Analysis

To answer questions regarding the drivers of C fluxes, we estimated generalized additive models (GAMs; Hastie & Tibshirani, 2017) using the mgcv package (Wood, 2017) and filtered, non-gap filled F_{CH4} daily data. Daily sums of fluxes were calculated based on days that had at least 32 half-hourly observations. GAMs are a form of generalized linear model where the response variable depends linearly on predictor variables via unknown smooth functions (Wood, 2006). This approach allows for non-linear behavior while maintaining comprehensibility. As an initial step in determining the best set of predictors in GAMs, Spearman correlation analyses for average daily NEE and F_{CH4}, versus all potential biotic and abiotic drivers were performed. Biophysical drivers of F_{CH4} and NEE such as T_{air}, T_{soil}, water level, air pressure, vapor pressure deficit (VPD), precipitation, GEE, and energy fluxes were explored. While the assumptions of GAMs (normality, homoscedasticity, and lack of autocorrelation in residuals) are satisfied using daily values of F_{CH4} in other wetland ecosystems (Yu et al., 2022), these assumptions were tested for our study site. Thin plate regression splines for smoothing functions of non-linear terms were used, as they are generally the optimal smoother for any given basis dimension (Wood, 2000), and these performed better compared to cubic regression, Gaussian, or soap film smooths. Basis dimensions (k) were checked with gam.check function, to evaluate terms for over-smoothing and lack of fit. When a low k-index was indicated, the k-value for the term was increased and reevaluated. A stepwise procedure was used to determine the optimal model, dropping the effect with the highest p-value sequentially, and ensuring that it resulted in improving performance with a lower AIC (Akaike Information Criterion) value. All statistical analyses were performed in R (version 4.3.2; R Core Team, 2023). Differences were considered significant at $p < 0.05$.

Following the novel method established by Rey-Sanchez et al. (2022), we generated footprint-weighted flux maps to detect spatial patterns or changes in F_{CH4} and NEE around the tower footprint by season. Footprint-weighted flux maps were estimated using MATLAB (version R2022a; The MathWorks Inc., 2022). Modeling of the footprint was completed using the K & M approach (Kormann & Meixner, 2001) using all daily observations with available filtered (un-gap-filled) data. Contouring was constructed to 50%, 60%, 70%, and 80% of plausible fluxes observed within tower footprint. Footprint contour data generated was saved as keyhole markup language (.kml) files readable in Google Earth Pro and heatmap images generated were stored as portable network graphics (.png).

3. Results

3.1. Environmental Conditions

Based on the cumulative anomaly approach, the wet season lengths for 2020 and 2021 were 187 and 175 days, respectively (Noska & Misra, 2016). In 2022, the site experienced a comparatively shorter wet season of 119 days (Table S2 in Supporting Information S1).

During the study, average daily T_{air} ranges were similar year over year. Dry season daily T_{air} ranges were 9.0–29.6°C, while wet season ranges trended higher as expected from 20.0 to 31.1°C (Figure 1a). Daily average soil temperature followed the same pattern as T_{air}, with wet season ranges from 24.1 to 32.7°C and dry season ranges slightly lower at 13.9–31.8°C (Figure 1b). Soil water potentials were near field capacity even during the dry season. Small pools persisted during dry periods, with the water table staying at or slightly above the surface. Water depth generally peaked during the late wet season period, at ∼0.2–0.4 m in depth (Figure 1c). The site received rainfall year-round, with the wet season typically responsible for nearly ∼70% of the mean annual precipitation (Figure 1f).

3.2. Ecosystem Fluxes

Annual totals of NEE were negative in the last 2 years of the study, pointing toward an increase in net uptake of CO_2 over the study period (Table S3 in Supporting Information S1). There was a ∼68% increase in CO_2 uptake from 2020 to 2021 (Table S3 in Supporting Information S1). This trend in carbon uptake continued from 2021 to 2022, when the site became a net sink. This was driven my gross photosynthesis at the site (Table S3 in Supporting Information S1). Daily mean fluxes of CH_4 varied each year, with 2020 and 2021 having the highest daily mean rates. Wet season CH_4 fluxes decreased each year such that 2022 was close to zero. There was no clear diurnal pattern in CH_4 fluxes. The annual average GCB ratio, calculated as daily CH_4 versus CO_2, decreased from 2020 to 2022, from 0.18 to −0.04 (Table S3 in Supporting Information S1). While GCB had no consistent trend year over year when examining seasonal averages (Table 1), GCB was notably lower during dry seasons compared to preceding wet seasons.

3.3. Drivers of Fluxes

The GAM explained 48% of the deviance in NEE. The daily mean PPFD, water level, wind velocity, and LE were significant predictors of NEE ($p < 0.05$), which varied by season (Table 2). Generally, as water level increased, respiration rates also decreased until an inflection point at ∼0.4 m, after which we observed increase of CO_2 efflux from the system (Figure 2c).

PPFD was found to have a significant relationship with NEE during the dry season, whereby low values of PPFD were associated with high positive fluxes (Figure 2b). During the dry season increasing windspeed led to positive fluxes of CO_2 (Figure 2e) The cosine of wind direction, indicating influence in the north-south direction was not a significant predictor of NEE and was removed from the models. Pressure and the sine of wind direction (east-west influence) were not found to be significant predictors (Figures 2d and 2f); however, the terms improved model deviance explained (∼7%), indicating that they contributed to explaining variance in NEE in conjunction with other variables, which may not be visible in a univariate sense. Latent energy was a strong predictor, indicating greater uptake of CO_2 with increasing LE in both seasons (Figure 2g). However, the model has substantial uncertainty with daily LE values above ∼7,000 w, values which are outside of the observed range for the dry season, as the dominant energy flux is sensible heat (H) during this time of year.

A different set of predictors were significant in the model of F_{CH4} ($p < 0.05$), which explained 19% of the variability in daily CH_4 fluxes (Table 2; Figure 3). T_{air} was a significant predictor of F_{CH4} during wet seasons, whereby higher temperatures led to lower F_{CH4} (Figure 3b). Soil temperature had a positive relationship with F_{CH4} during the dry and wet seasons (Figure 3a). The water level during the wet season had a significant non-linear relationship with F_{CH4}, whereby water levels about 0.2 m decreased F_{CH4} (Figure 3c). Daily average PPFD was a significant driver of F_{CH4} rates during the wet season (Figure 3d); when PPFD was above ∼200 µmol, it had a negative association with F_{CH4}, where water table depths >0.5 m may drive CH_4 uptake. R_{eco} approached significance ($p = 0.052$) during the wet season, with increasing R_{eco} leading to decreasing rates of F_{CH4} (Figure 3e). GEE was only a significant driver of F_{CH4} during the wet season. When GEE was

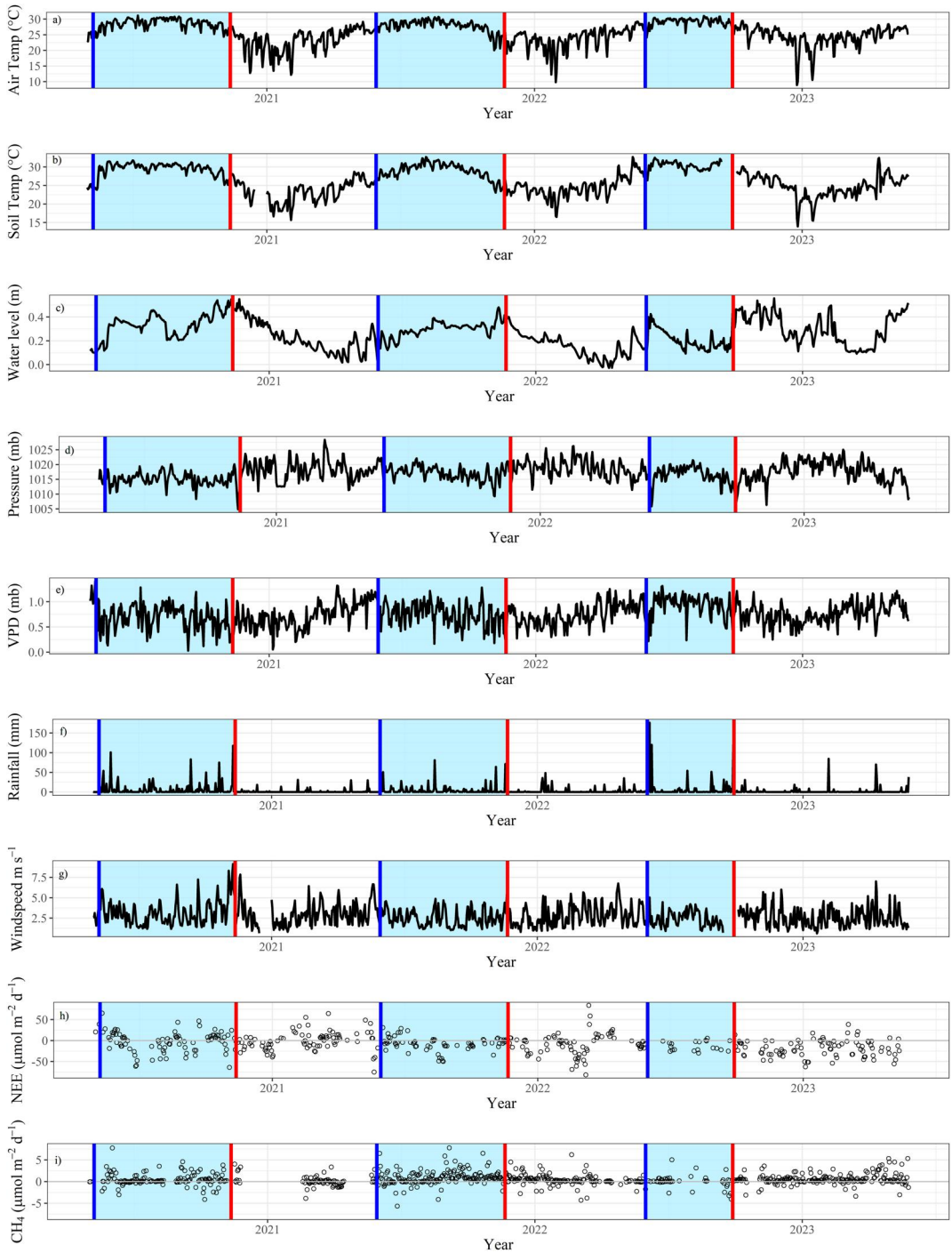

Figure 1. Average daily (a) air temperature, (b) soil temperature, (c) water level, (d) air pressure, (e) vapor pressure deficit, (f) rainfall, (g) windspeed, and filtered daily sums of (h) NEE, and (i) CH_4 fluxes for days with 32 or more observations (16 hr) at US-EvM. Vertical blue lines and shading indicate wet season; vertical red lines indicate the onset of dry season.

20–50 µmol m^{-2} d^{-1}, there was a slight increase in F_{CH4} release; however, when GEE was >50 µmol m^{-2} d^{-1} there was decreased F_{CH4} (Figure 3f). Rainfall during both seasons was a driver of F_{CH4}. During the wet season, daily rainfall events with >20 mm led to increasing CH_4 emissions (Figure 3g).

Table 1
Summary Statistics of Daily Fluxes of NEE, GEE, R_{eco}, and F_{CH4} (g C m^{-2})

Year	Season	NEE	GEE	R_{eco}	R_{eco}/GEE	RF_{CO2}	F_{CH4}	RF_{CH4}	GCB
2020	Wet	28.05	118.19	146.24	1.24	1.89	4.11	0.01	0.15
2020–2021	Dry	8.76	164.25	173.01	1.05	1.98	0.89	<0.01	0.10
2021	Wet	6.63	122.19	128.81	1.05	2.06	4.73	0.01	0.71
2021–2022	Dry	−23.81	175.57	151.76	0.86	2.15	3.50	0.01	−0.15
2022	Wet	−34.57	130.27	95.70	0.73	2.04	0.17	<0.01	0.00
2022–2023	Dry	−67.20	237.96	170.76	0.72	2.32	4.06	0.01	−0.06

Note. Mean daily net radiative forcing (RF, CO_2 as W m^{-2} ppm^{-1} and CH_4 as W m^{-2} ppb^{-1}) and greenhouse carbon balance (GCB, CH_4 g C m^{-2}/CO_2 g C m^{-2}). Based on gap-filled data set from meteorological measurements collected prior to the start of flux measurements.

3.4. Heatmap of NEE and CH_4

Daytime weighted heatmap models of NEE and F_{CH4} rates were produced for 80% of the plausible fluxes observed within the footprint of the tower using the K & M method. Footprint estimation indicated that 80% of observed fluxes occurred within approximately 185 m of the flux tower. For NEE, the model indicated increased uptake south of the tower that became more widespread each year during the study (Figure 4). The area south of the tower is dominated by red mangroves which are expanding in density and size. Regarding F_{CH4}, source fluxes seemingly varied year over year. In the first year of the study, modeling indicated the southeast of the tower as a source of CH_4 (Figure 4). However, this varied in subsequent years.

4. Discussion

Environmental conditions, especially tidal influences that can be exacerbated by tropical cyclones, play a role in reinforcing state change (Krauss & Osland, 2020; Osland, Feher, Anderson, et al., 2020). At our study site, red mangroves continued to proliferate over the study period, which was evident in the heatmap modeling. Water level, salinity, and rainfall were important factors that modulated seasonal CH_4 emissions. As this ecosystem develops and the mangroves continue their landward march, we anticipate a continued transition from net warming to a cooling radiative forcing.

4.1. Environmental Factors

The wet season length was consistent (~180 days; Table S2 in Supporting Information S1) during the study period apart from 2022, when it was just 119 days. Despite a shorter wet season in 2022, the succeeding dry season was impacted by a relatively active tropical cyclone season. While the SESE region did not receive any direct landfall of tropical cyclones during the study period, Hurricane Ian made landfall ~200 km north of the site as a category 4 storm in October 2022. We observed over 100 mm of precipitation during the period associated with this storm. Additionally, storm surge and timing of perigean spring tides led to increased water table depth during the event which lasted into the following month. Depending on the magnitude of future disturbances, we hypothesize that the transition to a mangrove forest at our study site would make it more resilient against future impact compared to its previous marsh state (Krauss & Osland, 2020; Osland et al., 2017; Zhang et al., 2018).

Reported values of the Southern Oscillation Index were positive for most of the study period (January 2020–April 2023) with early indications of the entry into an El Niño period in the near future (NOAA, 2023). This is important in the continuation of the mangrove forest as a C sink, as other Everglades studies have indicated wet season conditions during El Niño may drive increased CO_2 uptake and shorter dry seasons drive lower respiration (Malone et al., 2014). The length of the wet/dry season is also important in the timing of foliar abscission in *Rhizophora* as the onset of dry season promotes this strategy to reduce water stress (Fernandes et al., 2007; Freire et al., 2022). The interaction of salinity with hydroperiod length during these phases may also introduce an effect that we were not able to directly observe.

Table 2
Effective Degrees of Freedom (EDF), Reference Degrees of Freedom (RDF), F-Values, and p-Values for GAMs of NEE and F_{CH4}

Model	Effect	EDF	RDF	*F*-value	*p*-value
NEE	PPFD × dry	6.871	7.968	2.946	0.004*
	PPFD × wet	1.000	1.001	0.797	0.373
	T_{air} × dry	1.000	1.001	2.693	0.102
	T_{air} × wet	1.000	1.001	0.497	0.481
	Water level × dry	3.488	4.362	5.521	<0.001*
	Water level × wet	4.141	5.086	7.601	<0.001*
	Pressure × dry	2.577	3.298	1.176	0.284
	Pressure × wet	3.382	4.202	1.577	0.172
	Wind Velocity × dry	1.000	1.001	13.460	<0.001*
	Wind Velocity × wet	3.464	4.308	1.988	0.088
	sin (Wind Direction) × dry	1.988	2.455	1.272	0.348
	sin (Wind Direction) × wet	1.000	1.001	0.032	0.859
	LE × dry	4.047	4.986	12.952	<0.001*
	LE × wet	3.524	4.394	3.301	0.008*
CH_4	T_{soil} × dry	1.000	1.000	5.987	0.015*
	T_{soil} × wet	2.505	3.143	2.656	0.039*
	T_{air} × dry	3.143	3.946	1.178	0.305
	T_{air} × wet	1.000	1.000	7.005	0.008*
	Water level × dry	1.532	1.899	2.139	0.095
	Water level × wet	2.014	2.597	3.613	0.017*
	R_{eco} × dry	1.001	1.001	0.006	0.940
	R_{eco} × wet	1.000	1.000	3.785	0.052
	GEE × dry	3.105	3.941	2.218	0.079
	GEE × wet	4.904	5.976	2.081	0.047*
	PPFD × dry	1.000	1.000	0.023	0.880
	PPFD × wet	1.505	1.849	6.291	0.002*
	Rainfall × dry	2.083	2.565	3.468	0.020*
	Rainfall × wet	5.818	6.840	3.659	0.001*

Note. T_{air} = daily average air temperature (C), T_{soil} = daily average soil temperature 5–20 cm (C), PPFD = daily average Photosynthetic Photon Flux Density (μmol m^{-2} d^{-1}), R_{eco} = daily sum of ecosystem respiration (μmol m^{-2} d^{-1}), GEE = daily sum of gross ecosystem exchange (μmol m^{-2} d^{-1}); water level (m), latent energy (W m^{-2} d^{-1}), wind velocity $m^{-1}s^{-1}$, and wind direction are daily averages, precipitation (mm) is daily total, and "wet" or "dry" indicates meteorological season.

4.2. NEE

Red mangroves have continued to proliferate and colonize further landward at our study site. The expansion of the mangrove forest was evident in the heatmap modeling from 2020–2023, which showed increased areas of CO_2 uptake expanding throughout the tower footprint (Figure 4). Mangrove forest emergence has been shown to lead to increased leaf area and physiological activity in comparison to marsh plant species (Barr et al., 2009; Jimenez et al., 2012). Previous work has indicated that LAI can range from 3.0 to 5.7 among dwarf to basin mangrove forests (Araújo et al., 1997), which is dramatically higher than that observed in sawgrass-dominated ecosystems (~1.8; Schedlbauer et al., 2010). While maximum leaf-level photosynthetic rates (A_{max}) of 12.4–14.2 μmol CO_2 m^{-2} s^{-1} have been observed in sawgrass depending on wet or dry season conditions (Zhao et al., 2018), rates in red mangrove are reported between 5.3 and 9.9 μmol CO_2 m^{-2} s^{-1} (Cheeseman & Lovelock, 2004). When sawgrass is inundated and water levels rise, or faces salt stress, photosynthetic capacity declines significantly (Lamers et al., 2013; Zhao et al., 2018). Despite having lower rates of photosynthesis

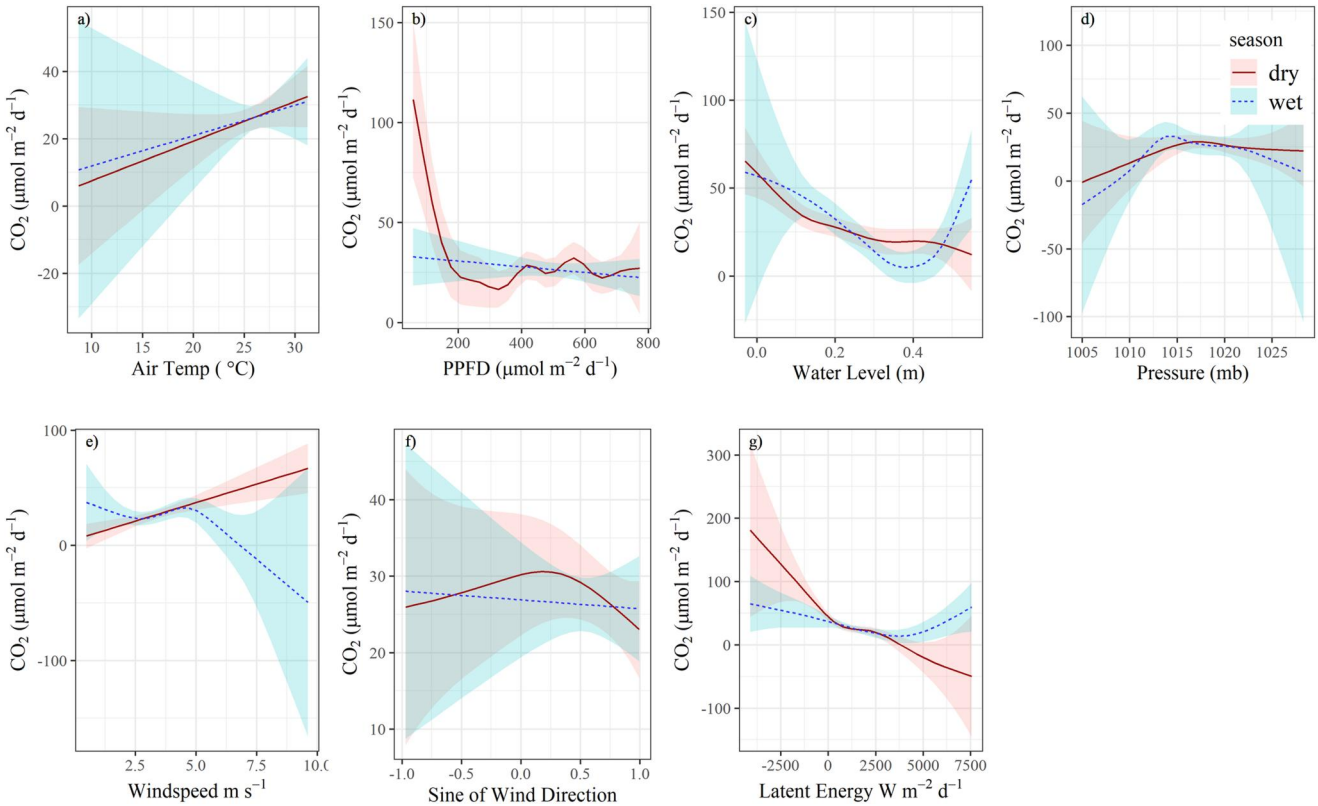

Figure 2. Estimated marginal means from GAMs of NEE at US-EvM by (a) T_{air}, (b) Photosynthetic Photon Flux Density, (c) water level, (d) air pressure, (e) windspeed, (f) wind direction, and (g) latent energy.

compared to other C_3 species, the rates for *R. mangle* remain largely unchanged during saline or inundated conditions compared to their marsh counterparts (Barr et al., 2010; Hogan et al., 2022; Lopes et al., 2023; Pezeshki et al., 1996; Zhao et al., 2021). Red mangroves' physiological adaptation to salt stress, along with the higher LAI, allows for greater carbon sequestration.

Mangroves also aid in stabilizing soils and likely lead to increased C burial (Breithaupt et al., 2012; Chen et al., 2017; Lunstrum & Chen, 2014; Xiong et al., 2018). As red mangroves are established, they offer greater stability control in C that is stored in peat with greater root production compared to marsh vegetation (Coldren et al., 2019). Other transitional sites in Florida with colonizing red mangroves have been reported to have soil C burial rates from 27 to 47 g C m^{-2} yr^{-1}, which is higher than those reported for marshes (4–7 g C m^{-2} yr^{-1}; Vaughn et al., 2020). While soil C burial contributes toward a small percentage of observed annual NEE, it is vital in expanding C capture and long-term retention. As mangroves mature and growth rates taper by comparison, soil carbon sequestration remains constant in mangrove forests, increasing carbon stocks (Walcker et al., 2018).

Water level also played a significant role in modulating productivity with increased depth (Smith et al., 2021). This result is likely due to inundation shifting microbial respiration to anaerobic pathways, but water level could also be affecting the physiological activity of red mangroves (Dang et al., 2019; Neubauer, 2013). The length of the hydroperiod or wet season can be important in controlling the productivity of *R. mangle* and could slow growth (Krauss et al., 2006). Extended periods of inundation may inhibit growth rates and add to plant stress with inundation driving increased leaf-level gas exchange as much as 0.1 μmol m^{-2} s^{-1} per 1 cm increase in water level (Hogan et al., 2022; McKee, 2011). Conversely, during the wet season, periods of flooding from hurricanes may also provide phosphorus (P), a limiting nutrient controlling productivity in mangrove forests, in an area that is generally associated with lower P availability (Castañeda-Moya et al., 2020). This would effectively fertilize the mangroves and drive increasing growth rates (Feller et al., 1994; Reef et al., 2010). While marine inputs of P would be the primary source during flooding, P input from sources further inland could also occur. Furthermore, as mangroves expand, the additional biomass will contribute to increased C

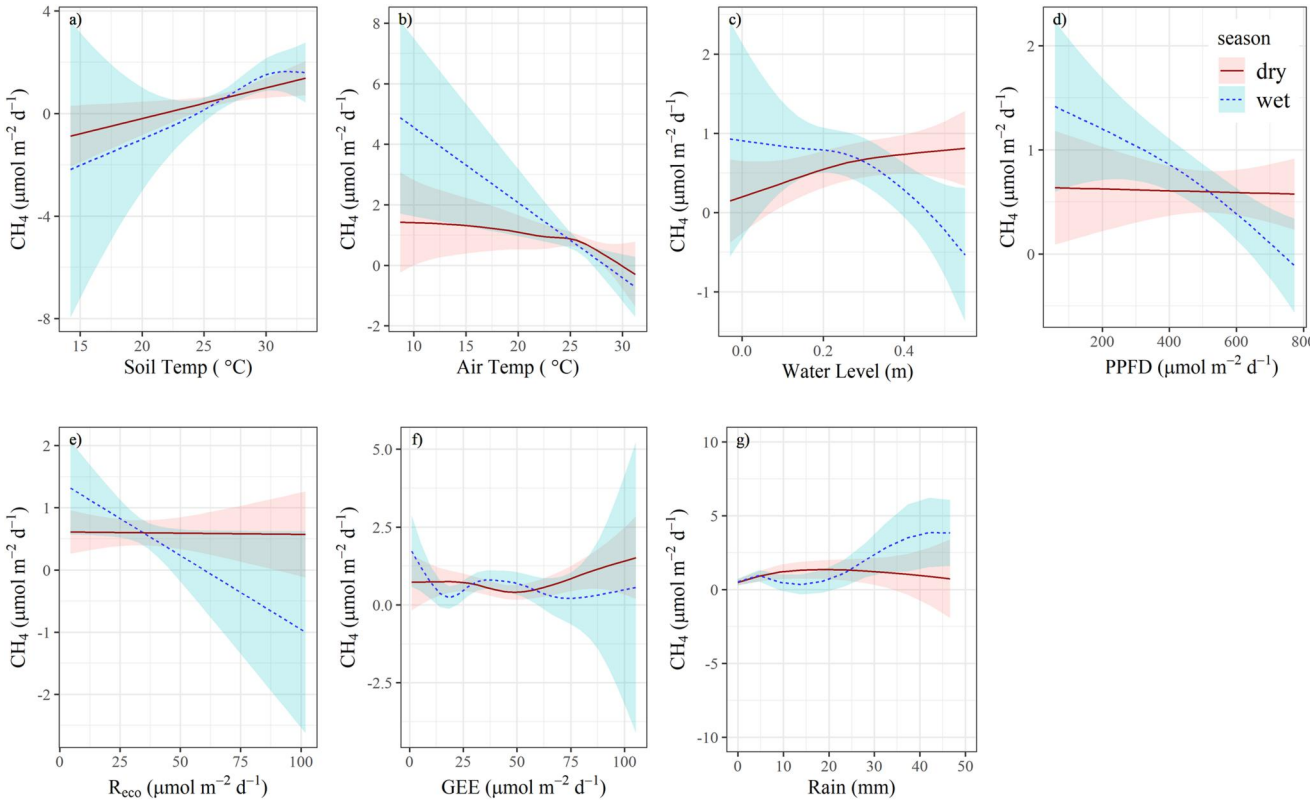

Figure 3. Estimated marginal means from GAMs of F_{CH_4} at US-EvM by: (a) T_{soil}, (b) T_{air}, (c) water level, (d) Photosynthetic Photon Flux Density, (e) R_{eco}, (f) GEE, (g) rainfall.

sequestration of the ecosystem (Castillo et al., 2017), a trend that we expect to persist as the site transitions to mangrove forest.

4.3. F_{CH_4}

Soil temperature was a key driver of methane emissions during both wet and dry seasons. These findings agree with previous studies where T_{soil} was a significant predictor of F_{CH4} in wetland systems (Irvin et al., 2021), whereby methanogens responded with higher metabolic activity when temperatures increased. Water level was only an important predictor of F_{CH4} during the wet season. The effect of spikes in porewater salinity during dry-down periods may drive an interaction that we were not able to directly measure. Saltwater contains sulfate, which in sufficient concentrations (>1 psu), causes sulfate-reducing bacteria to outcompete methanogens and dominate anaerobic respiration (DeBusk et al., 2015; Hackney & Avery, 2015; Orem et al., 2011). The interaction of inundation and salinity can drive rates of methanogenesis depending on the intensity of either condition (Vizza et al., 2017). Previous studies in the Everglades have demonstrated the importance of hydroperiod length as a driver of F_{CH4}, with periods of inundation leading to higher rates of CH_4 release (Yu et al., 2022). Ultimately, these patterns of salinity and hydroperiod will influence the C-sink capabilities of the developing mangrove forest (Odum et al., 1982). Rainfall was also a key driver of F_{CH4} during both seasons. Dry season major rainfall events (>20 mm day^{-1}) may have led to localized inundation, thus driving periods of enhanced anaerobic conditions. During periods of inundation throughout the year, rainfall may also drive off-gassing of dissolved CH_4 with surface agitation (Ho et al., 2018).

A majority of the methane fluxes in the system are likely from plant-mediated transport through aerenchyma (Jeffrey et al., 2019). There is less known on how the mangrove rhizosphere interacts with anaerobic processes that drive methanogenesis during this transitional period versus stressed *Cladium jamaicense*. Exudates from mangroves could prime microbial activity, leading to a potential lagged effect from photosynthesis that could

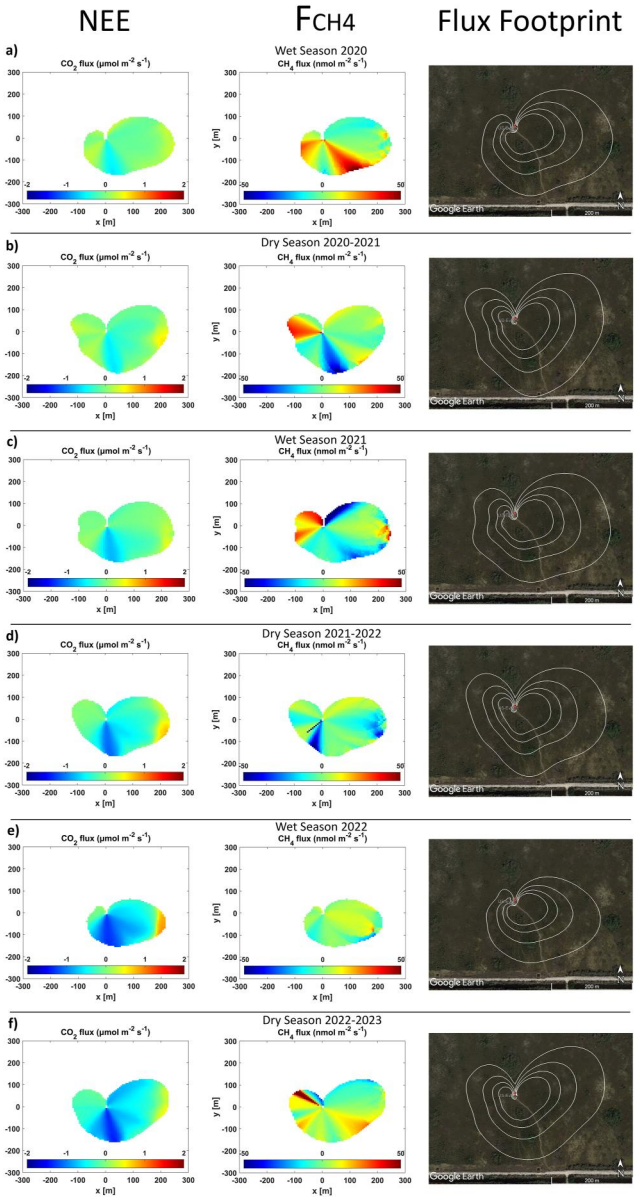

Figure 4. Heat map modeled to 50%–80% of plausible CO_2 and CH_4 fluxes measured in tower footprint. Cooler colors/more "blue" indicate negative fluxes and warmer/more "red" colors indicate positive fluxes.

drive F_{CH4} (Waldo et al., 2019). This interaction could be a potential explanation of the effect of PPFD on F_{CH4} during the wet season that was observed (Table 2).

Lastly, we observed benthic periphyton mats across the site, which likely contain both methanotrophs and methanogens (Jasrotia & Ogram, 2008). As mangroves establish and LAI increases we would expect a reduction in PPFD in the understory which could reduce benthic periphyton mats. Without these mats acting as a biogeochemical blanket and potentially oxidizing soil CH_4, there may be an increase in ebullition and release of CH_4 (Richardson et al., 2022). As the transition at the site continues, benthic periphyton assemblages will likely be shaded out as the mangrove forest expands. The assemblages would likely change in composition or become non-existent altogether and be replaced with a decomposing organic matter layer driven by mangrove leaf litter. This could impact the annual status of the ecosystem's radiative forcing and should be studied further.

4.4. Greenhouse Carbon Balance and Radiative Forcing

Global warming potentials (GWPs) are useful in comparing the overall carbon dynamics of the ecosystem and its ability to offset emissions. GCB estimates showed variability in the relative radiative forcing of CO_2 and CH_4 fluxes. In the first 2 years of this study, the system contributed to net atmospheric warming, which was likely due to a combination of declining sawgrass or an increase in sulfate. Then, as mangrove expansion increased (2022 and 2023), the area's GCB decreased below the greenhouse compensation point, leading to a cooling effect for both GWP_{20} and GWP_{100}. In addition to mangrove densities increasing, there was also a slight decrease in annual F_{CH4} emissions which contributed to a lower annual GCB ratio. This result could be due to sulfate from saltwater. Pulses of salinity can cause a muted effect on methanogenesis, as sulfate-reducers outcompete methanogens, leading to an increase in soil CO_2 and H_2S fluxes (Chambers et al., 2014; Wilson et al., 2018).

From previous studies of the Florida Coastal Everglades, short hydroperiod marshes have the potential to have a radiative cooling effect (Table 3), which is strongly determined by hydroclimatic patterns (Malone et al., 2014; Yu et al., 2022). However, marshes that stay inundated year-round with anaerobic soils, tend toward a net radiative heating effect (Whiting & Chanton, 2001). The initial hydrologic condition of our site —when sawgrass dominated— was likely nearly year-round inundation, and therefore before the initiated state change, we expected a positive GCB, similar to those of Everglades long hydroperiod marsh (US-Elm) (Table 3). In other EC studies, mature mangrove forests on the estuarine end of Shark River have been shown to have significantly higher annual uptake of CO_2 (Barr et al., 2012) driving a net cooling effect. Chamber-based studies in Everglades mangroves have also confirmed that these established forests have net cooling effects, with GCB ratios below the GWP_{20} and GWP_{100} thresholds (Cabezas et al., 2018).

Globally, mangrove forests have been shown to have a net cooling effect at both decadal and century-long timeframes (Table 3). To our knowledge, the highest fluxes from these systems showed F_{CH4} rates of 54.8 g C m^{-2} y^{-1} (Jha et al., 2014). Most mangrove forests, however, had lower emissions of CH_4, ranging from 6–15.6 g C m^{-2} y^{-1} (Gnanamoorthy et al., 2022; Liu et al., 2020). Additionally, this is accompanied by a much higher annual uptake of CO_2 (Table 4, Barr et al., 2012; Liu et al., 2020; Troxler et al., 2015). We expect that the site's trajectory of annual CH_4 emissions will stay well within reported annual means while CO_2 uptake will continue to increase.

Table 3
Previous Studies Examining Florida Coastal Everglades and Other Subtropical Mangrove Mean Annual Carbon Dynamics and Calculated Greenhouse Carbon Balance Ratios Based on Reported Fluxes

Site/Vegetation	CO_2 g C $m^{-2}y^{-1}$	CH_4 g C $m^{-2}y^{-1}$	GCB	Source
Coastal Everglades Sites				
US- Evm (Transitional Mangrove)	−6.62	9.27	−1.40	This study
US-Esm (Taylor Slough)	−42.7	125.7	−2.95	Jimenez et al. (2012), Malone et al. (2014), Yu et al. (2022)
US-Elm (Shark River Slough)	51.2	306.1	5.97	Jimenez et al. (2012), Malone et al. (2014), Yu et al. (2022)
US-Skr (Riverine Mangrove)	−998.4	–	–	Barr et al. (2013)
Naples Bay (Riverine Mangrove)	–	0.30[a]	–	Cabezas et al. (2018)
Other subtropical mangrove forest				
Mai Po Estuarine Mangroves	−782.3	11.7	−0.01	Liu et al. (2020)
Sundarbans Mangroves	249.0	54.8	0.22	Jha et al. (2014), Rodda et al. (2016)
Cauvery Vellar-Coleroon estuarine mangroves—Annual	183	–	–	Gnanamoorthy et al. (2020, 2022)
Wet (Oct.–Dec.)	115.2	15.6	0.14	
Dry (Apr.–June)	−4.50	6.0	−1.33	

[a]Denotes Chamber-Based Measurements, all Other Studies Utilize Eddy-Covariance Techniques.

We predict that as the mangrove forest in this study matures, the ecosystem will trend toward a persistent state of negative radiative forcing into the next century, assuming our site US-Evm remains undisturbed by tropical cyclones and can continue to mature (Twilley et al., 1999). At the maturation point, we expect that the forest peat level will increase, reaching similar concentrations observed in adjacent systems (Osland, Feher, Spivak, et al., 2020). Additionally, a mature stand will ultimately be more resilient and able to withstand defoliation and isolated mortality. With encroaching salinity from saltwater intrusion and pulse flooding, mangroves have been shown to activate salt-regulating genes to tolerate high salinity (~25 psu) and perform photosynthetic maintenance (Lopes et al., 2023). Both factors will ultimately determine the intensity of the net cooling effect provided by maturing mangrove forests in the future. It should be noted that our findings may be specific to freshwater marshes that exist on marl soils and may not be reflective of areas that are dominated by peat soils. In previous studies performed in peat dominated marshes, increased salinity was found to reduce sawgrass physiological activity and productivity due to changes in soil ion capacity which led to osmotic stress (Tully et al., 2019). This ultimately leads to a decrease in root biomass, making soils less stable (Wilson et al., 2018). Flooding also brings increased marine nutrients into wetlands, which change microbial activity, and when coupled with increased salinity causes peat collapse and release of stored carbon (Steinmuller et al., 2019). This peat collapse may lead to an opening for mangroves to establish or the formation of open water where vegetation is nonexistent. Additional research is still needed to understand the complex interaction between mangrove establishment and peat collapse.

5. Conclusions

In a coastal marsh transitioning to a mangrove forest, we observed seasonal variation in NEE with dry seasons markedly higher than the preceding wet season. Observed fluxes of CO_2 and CH_4 show that there is a decreasing trend in net radiative forcing from our site. Despite coastal marshes facing disturbances such as saltwater flooding, the transition to a mangrove forest continues to increase C sequestration capacity in the area. This highlights the important role mangrove establishment may play as a natural climate change solution to mitigate rising atmospheric CO_2 concentrations.

Our study provides new insight into the inland expansion of mangroves into areas that were previously freshwater coastal marshes. The current understanding of coastal wetland carbon dynamics has been well-documented for the poleward expansion of the species (Alongi, 2020; Osland et al., 2017). However, increasing sea level rise along with increasing storm surges caused by more intense tropical storms may accelerate the expansion of

mangroves inland. This could have significant implications for ecosystem composition, regional carbon dynamics, and radiative forcing.

We also argue that future research is needed to understand the spatial heterogeneity of CH_4 dynamics and in particular the complex interactions among benthic periphyton, soil microbiota, and colonizing mangroves. Investigating the roles of methanogens and methanotrophs within benthic periphyton mats and the rhizospheres of mangroves will aid in understanding the biogeochemical processes in play in these transitional ecosystems. While this transitional mangrove forest will likely continue to exhibit carbon dynamics in the range of the ecotone and mangrove ecosystems, our study demonstrated that there is still uncertainty in the face of natural disturbances. These transitioning ecosystems will occupy a unique niche in the carbon cycle that will continue to expand with climate change, underscoring the need for ongoing research to inform conservation and land management strategies that improve the broader climate change outcomes of these resilient ecosystems.

Data Availability Statement

Eddy covariance data and corresponding micrometeorological data are archived through the Ameriflux repository. Us-EvM (https://doi.org/10.17190/AMF/2229155) (Starr & Oberbuer, 2023).

Acknowledgments

All research was performed under permits issued by Everglades National Park (EVER-2009-SCI- 0070 and EVER-2013-SCI-0058). The authors would like to acknowledge the excellent support provided by the Florida Coastal Everglades Long Term Ecological Research Program (FCE-LTER) and the Southeast Environmental Research Center in the Institute of Water and Environment at Florida International University. This manuscript is partly based upon work supported by the National Science Foundation (NSF) through the FCE-LTER program under Grant DEB-1237517. This research is also based in part on support from the Department of Energy's (DOE) National Institute for Climate Change Research through Grant 07-SC-NICCR-1059 and the NSF Division of Atmospheric & Geospace Sciences Atmospheric Chemistry Program awards 1561139, 1233006, 1801310, and 1807533. National Science Foundation Graduate Research Fellowship Program, fellow 2023348536 and the Alabama Water Institute. Any opinions, findings, and conclusions or recommendations expressed in this material are those of the authors and do not necessarily reflect the views of FCE-LTER, NSF, or DOE.

References

Alongi, D. M. (2020). Carbon balance in salt marsh and mangrove ecosystems: A global synthesis. *Journal of Marine Science and Engineering*, *8*(10), 1–21. https://doi.org/10.3390/jmse8100767

Araújo, R. J., Jaramillo, J. C., & Snedaker, S. C. (1997). LAI and leaf size differences in two red mangrove forest types in south Florida. *Bulletin of Marine Science*, *60*(3), 643–647.

Ball, M. C. (1988). Ecophysiology of mangroves. *Trees*, *2*(3), 129–142. https://doi.org/10.1007/BF00196018

Barr, J. G., Engel, V., Fuentes, J. D., Fuller, D. O., & Kwon, H. (2013). Modeling light use efficiency in a subtropical mangrove forest equipped with CO2 eddy covariance. *Biogeosciences*, *10*(3), 2145–2158. https://doi.org/10.5194/bg-10-2145-2013

Barr, J. G., Engel, V., Fuentes, J. D., Zieman, J. C., O'Halloran, T. L., Smith, T. J., & Anderson, G. H. (2010). Controls on mangrove forest-atmosphere carbon dioxide exchanges in western Everglades National Park. *Journal of Geophysical Research*, *115*(G2), n/a-n/a. https://doi.org/10.1029/2009jg001186

Barr, J. G., Engel, V., Smith, T. J., & Fuentes, J. D. (2012). Hurricane disturbance and recovery of energy balance, CO 2 fluxes and canopy structure in a mangrove forest of the Florida Everglades. *Agricultural and Forest Meteorology*, *153*, 54–66. https://doi.org/10.1016/j.agrformet.2011.07.022

Barr, J. G., Fuentes, J. D., Engel, V., & Zieman, J. C. (2009). Physiological responses of red mangroves to the climate in the Florida Everglades. *Journal of Geophysical Research*, *114*(2). https://doi.org/10.1029/2008JG000843

Breithaupt, J. L., Smoak, J. M., Smith, T. J., Sanders, C. J., & Hoare, A. (2012). Organic carbon burial rates in mangrove sediments: Strengthening the global budget. *Global Biogeochemical Cycles*, *26*(3), 1–11. https://doi.org/10.1029/2012GB004375

Cabezas, A., Mitsch, W. J., MacDonnell, C., Zhang, L., Bydałek, F., & Lasso, A. (2018). Methane emissions from mangrove soils in hydrologically disturbed and reference mangrove tidal creeks in southwest Florida. *Ecological Engineering*, *114*, 57–65. https://doi.org/10.1016/j.ecoleng.2017.08.041

Castañeda-Moya, E., Rivera-Monroy, V. H., Chambers, R. M., Zhao, X., Lamb-Wotton, L., Gorsky, A., et al. (2020). Hurricanes fertilize mangrove forests in the Gulf of Mexico (Florida Everglades, USA). *Proceedings of the National Academy of Sciences of the United States of America*, *117*(9), 4831–4841. https://doi.org/10.1073/pnas.1908597117

Castillo, J. A. A., Apan, A. A., Maraseni, T. N., & Salmo, S. G. (2017). Estimation and mapping of above-ground biomass of mangrove forests and their replacement land uses in the Philippines using Sentinel imagery. *ISPRS Journal of Photogrammetry and Remote Sensing*, *134*, 70–85. https://doi.org/10.1016/j.isprsjprs.2017.10.016

Chambers, L. G., Davis, S. E., Troxler, T., Boyer, J. N., Downey-Wall, A., & Scinto, L. J. (2014). Biogeochemical effects of simulated sea level rise on carbon loss in an Everglades mangrove peat soil. *Hydrobiologia*, *726*(1), 195–211. https://doi.org/10.1007/s10750-013-1764-6

Cheeseman, J. M., & Lovelock, C. E. (2004). Photosynthetic characteristics of dwarf and fringe Rhizophora mangle L. in a Belizean mangrove. *Plant, Cell and Environment*, *27*(6), 769–780. https://doi.org/10.1111/j.1365-3040.2004.01181.x

Chen, G., Azkab, M. H., Chmura, G. L., Chen, S., Sastrosuwondo, P., Ma, Z., et al. (2017). Mangroves as a major source of soil carbon storage in adjacent seagrass meadows. *Scientific Reports*, *7*, 1–10. https://doi.org/10.1038/srep42406

Clark, K. L., Gholz, H. L., Moncrieff, J. B., Cropley, F., & Loescher, H. W. (1999). Environmental controls over net exchanges of carbon dioxide from contrasting Florida ecosystems. *Ecological Applications*, *9*(3), 936–948. https://doi.org/10.1890/1051-0761(1999)009[0936:ECONEO]2.0.CO;2

Coldren, G. A., Langley, J. A., Feller, I. C., & Chapman, S. K. (2019). Warming accelerates mangrove expansion and surface elevation gain in a subtropical wetland. *Journal of Ecology*, *107*(1), 79–90. https://doi.org/10.1111/1365-2745.13049

Costanza, R., D'Arge, R., de Groot, R., Farber, S., Grasso, M., Hannon, B., et al. (1997). The value of the world's ecosystem services and natural capital. LK -. *Ecological Economics*, *387*(6630), 253–260. Nature TA - TT -. https://doi.org/10.1016/s0921-8009(98)00020-2

Dang, C., Morrissey, E. M., Neubauer, S. C., & Franklin, R. B. (2019). Novel microbial community composition and carbon biogeochemistry emerge over time following saltwater intrusion in wetlands. *Global Change Biology*, *25*(2), 549–561. https://doi.org/10.1111/gcb.14486

Davis, S., & Ogden, J. C. (1994). *Everglades: The ecosystem and its restoration*. CRC Press.

Day, J. W., Christian, R. R., Boesch, D. M., Yáñez-Arancibia, A., Morris, J., Twilley, R. R., et al. (2008). Consequences of climate change on the ecogeomorphology of coastal wetlands. *Estuaries and Coasts*, *31*(3), 477–491. https://doi.org/10.1007/s12237-008-9047-6

DeBusk, T. A., Dierberg, F. E., DeBusk, W. F., Jackson, S. D., Potts, J. A., Galloway, S. C., et al. (2015). Sulfide concentration effects on Typha domingensis Pers. (cattail) and Cladium jamaicense Crantz (sawgrass) growth in Everglades marshes. *Aquatic Botany*, *124*, 78–84. https://doi.org/10.1016/j.aquabot.2015.03.006

Egler, F. E. (1952). Southeast saline Everglades vegetation, Florida and its management – With 16 figs., 8 photographs, 4 plates and 1 table. *Vegetatio Acta Geobotanica*, *3*(4–5), 213–265. https://doi.org/10.1007/BF00539820

Feller, I. C., Mckee, K. L., Whigham, D., & O'Neill, J. (1994). Nitrogen vs. phosphorus limitation across an ecotonal gradient in a mangrove forest. *Quaternary International*, *24*(C), 17–23. https://doi.org/10.1023/A:1021166010892

Fernandes, M. E. B., Nascimento, A. A. M. d., & Carvalho, M. L. (2007). Estimativa da produção anual de serapilheira dos bosques de mangue no Furo Grande, Bragança-Pará. *Revista Árvore*, *31*(5), 949–958. https://doi.org/10.1590/s0100-67622007000500019

Foken, T., & Leclerc, M. Y. (2004). Methods and limitations in validation of footprint models. *Agricultural and Forest Meteorology*, *127*(3–4), 223–234. https://doi.org/10.1016/j.agrformet.2004.07.015

Foken, T., & Wichura, B. (1996). Tools for quality assessment of surface-based flux measurements. *Agricultural and Forest Meteorology*, *78*(1–2), 83–105. https://doi.org/10.1016/0168-1923(95)02248-1

Fratini, G., & Mauder, M. (2014). Towards a consistent eddy-covariance processing: An intercomparison of EddyPro and TK3. *Atmospheric Measurement Techniques*, *7*(7), 2273–2281. https://doi.org/10.5194/amt-7-2273-2014

Freire, A. S. C., Vitorino, M. I., de Souza, A. M. L., & Germano, M. F. (2022). Analysis of the energy balance and CO2 flow under the influence of the seasonality of climatic elements in a mangrove ecosystem in Eastern Amazon. *International Journal of Biometeorology*, *66*(4), 647–659. https://doi.org/10.1007/s00484-021-02224-8

Gnanamoorthy, P., Chakraborty, S., Nagarajan, R., Ramasubramanian, R., Selvam, V., Burman, P. K. D., et al. (2022). Seasonal variation of methane fluxes in a mangrove ecosystem in South India: An eddy covariance-based approach. *Estuaries and Coasts*, *45*(2), 551–566. https://doi.org/10.1007/s12237-021-00988-1

Gnanamoorthy, P., Selvam, V., Deb Burman, P. K., Chakraborty, S., Karipot, A., Nagarajan, R., et al. (2020). Seasonal variations of net ecosystem (CO2) exchange in the Indian tropical mangrove forest of Pichavaram. *Estuarine, Coastal and Shelf Science*, *243*(June), 106828. https://doi.org/10.1016/j.ecss.2020.106828

Goulden, M. L., Munger, J. W., Fan, S. M., Daube, B. C., & Wofsy, S. C. (1996). Measurements of carbon sequestration by long-term eddy covariance: Methods and a critical evaluation of accuracy. *Global Change Biology*, *2*(3), 169–182. https://doi.org/10.1111/j.1365-2486.1996.tb00070.x

Hackney, C. T., & Avery, G. B. (2015). Tidal wetland community response to varying levels of flooding by saline water. *Wetlands*, *35*(2), 227–236. https://doi.org/10.1007/s13157-014-0597-z

Hastie, T. J., & Tibshirani, R. J. (2017). *Generalized additive models* (1st ed.). Routledge. https://doi.org/10.1201/9780203753781

Helbig, M., Chasmer, L. E., Kljun, N. C., Quinton, W. L., Treat, C. C., & Sonnentag, O. (2017). The positive net radiative greenhouse gas forcing of increasing methane emissions from a thawing boreal forest-wetland landscape. *Global Change Biology*, *23*(6), 2413–2427. https://doi.org/10.1111/gcb.13520

Herbert, E. R., Boon, P., Burgin, A. J., Neubauer, S. C., Franklin, R. B., Ardon, M., et al. (2015). A global perspective on wetland salinization: Ecological consequences of a growing threat to freshwater wetlands. *Ecosphere*, *6*(10), 1–43. https://doi.org/10.1890/ES14-00534.1

Ho, D. T., Engel, V. C., Ferrón, S., Hickman, B., Choi, J., & Harvey, J. W. (2018). On factors influencing air-water gas exchange in emergent wetlands. *Journal of Geophysical Research: Biogeosciences*, *123*(1), 178–192. https://doi.org/10.1002/2017JG004299

Hogan, J. A., Castañeda-Moya, E., Lamb-Wotton, L., Troxler, T., & Baraloto, C. (2022). Water levels primarily drive variation in photosynthesis and nutrient use of scrub Red Mangroves in the southeastern Florida Everglades. *Tree Physiology*, *42*(4), 797–814. https://doi.org/10.1093/treephys/tpab151

Huang, J., Mendoza, B., Daniel, J. S., Nielsen, C. J., Rotstayn, L., & Wild, O. (2013). Anthropogenic and natural radiative forcing. *Climate Change 2013 the Physical Science Basis: Working Group I Contribution to the Fifth Assessment Report of the Intergovernmental Panel on Climate Change*, 659–740. https://doi.org/10.1017/CBO9781107415324.018

Irvin, J., Zhou, S., McNicol, G., Lu, F., Liu, V., Fluet-Chouinard, E., et al. (2021). Gap-filling eddy covariance methane fluxes: Comparison of machine learning model predictions and uncertainties at FLUXNET-CH4 wetlands. *Agricultural and Forest Meteorology*, *308–309*, 308–309. https://doi.org/10.1016/j.agrformet.2021.108528

Jasrotia, P., & Ogram, A. (2008). Diversity of nifH genotypes in floating periphyton mats along a nutrient gradient in the Florida everglades. *Current Microbiology*, *56*(6), 563–568. https://doi.org/10.1007/s00284-008-9124-x

Jeffrey, L. C., Maher, D. T., Johnston, S. G., Kelaher, B. P., Steven, A., & Tait, D. R. (2019). Wetland methane emissions dominated by plant-mediated fluxes: Contrasting emissions pathways and seasons within a shallow freshwater subtropical wetland. *Limnology & Oceanography*, *64*(5), 1895–1912. https://doi.org/10.1002/lno.11158

Jha, C. S., Rodda, S. R., Thumaty, K. C., Raha, A. K., & Dadhwal, V. K. (2014). Eddy covariance based methane flux in Sundarbans mangroves, India. *Journal of Earth System Science*, *123*(5), 1089–1096. https://doi.org/10.1007/s12040-014-0451-y

Jiang, J., DeAngelis, D. L., Anderson, G. H., & Smith, T. J. (2014). Analysis and simulation of propagule dispersal and salinity intrusion from storm surge on the movement of a marsh-mangrove ecotone in south Florida. *Estuaries and Coasts*, *37*(1), 24–35. https://doi.org/10.1007/s12237-013-9666-4

Jimenez, K. L., Starr, G., Staudhammer, C. L., Schedlbauer, J. L., Loescher, H. W., Malone, S. L., & Oberbauer, S. F. (2012). Carbon dioxide exchange rates from short- and long-hydroperiod Everglades freshwater marsh. *Journal of Geophysical Research*, *117*(G4). https://doi.org/10.1029/2012JG002117

Kormann, R., & Meixner, F. X. (2001). An analytical footprint model for non-neutral stratification. *Boundary-Layer Meteorology*, *99*(2), 207–224. https://doi.org/10.1023/A:1018991015119

Krauss, K. W., Doyle, T. W., Twilley, R. R., Rivera-Monroy, V. H., & Sullivan, J. K. (2006). Evaluating the relative contributions of hydroperiod and soil fertility on growth of south Florida mangroves. *Hydrobiologia*, *569*(1), 311–324. https://doi.org/10.1007/s10750-006-0139-7

Krauss, K. W., & Osland, M. J. (2020). Tropical cyclones and the organization of mangrove forests: A review. *Annals of Botany*, *125*(2), 213–234. https://doi.org/10.1093/aob/mcz161

Lamers, L. P. M., Govers, L. L., Janssen, I. C. J. M., Geurts, J. J. M., Van der Welle, M. E. W., Van Katwijk, M. M., et al. (2013). Sulfide as a soil phytotoxin—A review. *Frontiers in Plant Science*, *4*(JUL), 1–14. https://doi.org/10.3389/fpls.2013.00268

Liaw, A., & Wiener, M. (2002). Classification and regression by randomForest. *R News*, *2*(3), 18–22. Retrieved from https://cran.r-project.org/doc/Rnews/

Liu, J., Zhou, Y., Valach, A., Shortt, R., Kasak, K., Rey-Sanchez, C., et al. (2020). Methane emissions reduce the radiative cooling effect of a subtropical estuarine mangrove wetland by half. *Global Change Biology*, *26*(9), 4998–5016. https://doi.org/10.1111/gcb.15247

Lopes, D. M. d. S., Lopes, A. d. S., Falqueto, A. R., Gontijo, A. B. P. L., Rogalski, M., & Tognella, M. M. P. (2023). Photosynthetic and gene expression analyses in Rhizophora mangle L. plants growing in field conditions provide insights into adaptation to high-salinity environments. *Trees - Structure and Function*, *37*(3), 733–747. https://doi.org/10.1007/s00468-022-02380-3

Lunstrum, A., & Chen, L. (2014). Soil carbon stocks and accumulation in young mangrove forests. *Soil Biology and Biochemistry*, *75*, 223–232. https://doi.org/10.1016/j.soilbio.2014.04.008

Malone, S. L., Staudhammer, C. L., Oberbauer, S. F., Olivas, P., Ryan, M. G., Schedlbauer, J. L., et al. (2014). El Niño Southern Oscillation (ENSO) enhances CO2 exchange rates in freshwater marsh ecosystems in the Florida Everglades. *PLoS One*, *9*(12), 1–30. https://doi.org/10.1371/journal.pone.0115058

McDermitt, D., Burba, G., Xu, L., Anderson, T., Komissarov, A., Riensche, B., et al. (2011). A new low-power, open-path instrument for measuring methane flux by eddy covariance. *Applied Physics B: Lasers and Optics*, *102*(2), 391–405. https://doi.org/10.1007/s00340-010-4307-0

McKee, K. L. (2011). Biophysical controls on accretion and elevation change in Caribbean mangrove ecosystems. *Estuarine, Coastal and Shelf Science*, *91*(4), 475–483. https://doi.org/10.1016/j.ecss.2010.05.001

Mitsch, W. J., Bernal, B., Nahlik, A. M., Mander, Ü., Zhang, L., Anderson, C. J., et al. (2013). Wetlands, carbon, and climate change. *Landscape Ecology*, *28*(4), 583–597. https://doi.org/10.1007/s10980-012-9758-8

Myhre, G., Highwood, E. J., Shine, K. P., & Stordal, F. (1998). New estimates of radiative forcing due to well mixed greenhouse gases. *Geophysical Research Letters*, *25*(14), 2715–2718. https://doi.org/10.1029/98GL01908

National Climatic Data Center. (2023). No title. Retrieved from www.ncdc.noaa.gov

Neubauer, S. C. (2013). Ecosystem responses of a tidal freshwater marsh experiencing saltwater intrusion and altered hydrology. *Estuaries and Coasts*, *36*(3), 491–507. https://doi.org/10.1007/s12237-011-9455-x

NOAA. (2023). Southern oscillation index. Retrieved from https://www.cpc.ncep.noaa.gov/data/indices/soi

Noska, R., & Misra, V. (2016). Characterizing the onset and demise of the Indian summer monsoon. *Geophysical Research Letters*, *43*(9), 4547–4554. https://doi.org/10.1002/2016GL068409

Odum, W., McIvor, C., & Smith, T. J. (1982). The ecology of the mangroves of south Florida: A community profile. The Service.

Orem, W., Gilmour, C., Axelrad, D., Krabbenhoft, D., Scheidt, D., Kalla, P., et al. (2011). Sulfur in the South Florida ecosystem: Distribution, sources, biogeochemistry, impacts, and management for restoration. *Critical Reviews in Environmental Science and Technology*, *41*(SUPPL. 1), 249–288. https://doi.org/10.1080/10643389.2010.531201

Osland, M. J., Day, R. H., Hall, C. T., Brumfield, M. D., Dugas, J. L., & Jones, W. R. (2017). Mangrove expansion and contraction at a poleward range limit: Climate extremes and land-ocean temperature gradients. *Ecology*, *98*(1), 125–137. https://doi.org/10.1002/ecy.1625

Osland, M. J., Feher, L. C., Anderson, G. H., Vervaeke, W. C., Krauss, K. W., Whelan, K. R. T., et al. (2020). A tropical cyclone-induced ecological regime shift: Mangrove forest conversion to mudflat in Everglades National Park (Florida, USA). *Wetlands*, *40*(5), 1445–1458. https://doi.org/10.1007/s13157-020-01291-8

Osland, M. J., Feher, L. C., Griffith, K. T., Cavanaugh, K. C., Enwright, N. M., Day, R. H., et al. (2017). Climatic controls on the global distribution, abundance, and species richness of mangrove forests. *Ecological Monographs*, *87*(2), 341–359. https://doi.org/10.1002/ecm.1248

Osland, M. J., Feher, L. C., Spivak, A. C., Nestlerode, J. A., Almario, A. E., Cormier, N., et al. (2020). Rapid peat development beneath created, maturing mangrove forests: Ecosystem changes across a 25-yr chronosequence. *Ecological Applications*, *30*(4), 1–12. https://doi.org/10.1002/eap.2085

Pezeshki, S. R., DeLaune, R. D., Kludze, H., & Choi, H. S. (1996). Photosynthetic and growth responses of cattail (*Typha domingensis*) and sawgrass (*Cladium jamaicense*) to soil redox conditions. *Aquatic Botany*, *54*(1), 25–35. https://doi.org/10.1016/0304-3770(96)01033-9

R Core Team. (2023). R: A language and environment for statistical computing. R Foundation for Statistical Computing. Retrieved from https://www.R-project.org/

Reddy, K. R., & DeLaune, R. D. (2008). Biogeochemistry of wetlands.

Reef, R., Feller, I. C., & Lovelock, C. E. (2010). Nutrition of mangroves. *Tree Physiology*, *30*(9), 1148–1160. https://doi.org/10.1093/treephys/tpq048

Rey-sanchez, C., Arias-ortiz, A., Kasak, K., & Chu, H. (2022). Detecting hot spots of methane flux using footprint-weighted flux maps (pp. 1–22). https://doi.org/10.1029/2022JG006977

Richardson, C. J. (2010). The Everglades: North America's subtropical wetland. *Wetlands Ecology and Management*, *18*(5), 517–542. https://doi.org/10.1007/s11273-009-9156-4

Richardson, W. P., Reba, M. L., & Runkle, B. R. K. (2022). Modification of a wavelet-based method for detecting ebullitive methane fluxes in eddy-covariance observations: Application at two rice fields. *Boundary-Layer Meteorology*, *184*(1), 71–111. https://doi.org/10.1007/s10546-022-00703-y

Rodda, S. R., Thumaty, K. C., Jha, C. S., & Dadhwal, V. K. (2016). Seasonal variations of carbon dioxide, water vapor and energy fluxes in tropical Indian mangroves. *Forests*, *7*(2), 1–18. https://doi.org/10.3390/f7020035

Ross, M. S., Meeder, J. F., Sah, J. P., Ruiz, P. L., & Telesnicki, G. J. (2000). The Southeast Saline Everglades revisited: 50 years of coastal vegetation change. *Journal of Vegetation Science*, *11*(1), 101–112. https://doi.org/10.2307/3236781

Ross, M. S., Stoffella, S. L., Vidales, R., Meeder, J. F., Kadko, D. C., Scinto, L. J., et al. (2022). Sea-level rise and the persistence of tree islands in coastal landscapes. *Ecosystems*, *25*(3), 586–602. https://doi.org/10.1007/s10021-021-00673-1

Schedlbauer, J. L., Oberbauer, S. F., Starr, G., & Jimenez, K. L. (2010). Seasonal differences in the CO2 exchange of a short-hydroperiod Florida Everglades marsh. *Agricultural and Forest Meteorology*, *150*(7–8), 994–1006. https://doi.org/10.1016/j.agrformet.2010.03.005

Smith, R. S., Beauvais, J., & Byers, J. E. (2021). Traits of resident saltmarsh plants promote retention of range-expanding mangroves under specific tidal regimes. *Estuaries and Coasts*, *45*(Bruno 2000), 1422–1433. https://doi.org/10.1007/s12237-021-01016-y

Starr, G., & Oberbuer, S. F. (2023). AmeriFlux BASE US-EvM everglades saltwater intrusion marsh, ver. 1-5. (Dataset). AmeriFlux AMP. https://doi.org/10.17190/AMF/2229155

Staudhammer, C. L., Malone, S. L., Zhao, J., Yu, Z., Starr, G., & Oberbauer, S. F. (2022). Methane emissions from subtropical wetlands: An evaluation of the role of data filtering on annual methane budgets. *Agricultural and Forest Meteorology*, *321*(October 2021), 108972. https://doi.org/10.1016/j.agrformet.2022.108972

Steinmuller, H. E., Dittmer, K. M., White, J. R., & Chambers, L. G. (2019). Understanding the fate of soil organic matter in submerging coastal wetland soils: A microcosm approach. *Geoderma*, *337*, 1267–1277. https://doi.org/10.1016/j.geoderma.2018.08.020

Steinmuller, H. E., Stoffella, S. L., Vidales, R., Ross, M. S., Dattamudi, S., & Scinto, L. J. (2021). Characterizing hydrologic effects on soil physicochemical variation within tree islands and marshes in the coastal Florida Everglades. *Soil Science Society of America Journal*, *85*(4), 1269–1280. https://doi.org/10.1002/saj2.20270

Sternberg, L. D. S. L., Teh, S. Y., Ewe, S. M. L., Miralles-Wilhelm, F., & DeAngelis, D. L. (2007). Competition between hardwood hammocks and mangroves. *Ecosystems*, *10*(4), 648–660. https://doi.org/10.1007/s10021-007-9050-y

The MathWorks Inc. (2022). MATLAB version: 9.13.0 (R2022b). The MathWorks Inc. Retrieved from https://www.mathworks.com

Troxler, T. G., Barr, J. G., Fuentes, J. D., Engel, V., Anderson, G., Sanchez, C., et al. (2015). Component-specific dynamics of riverine mangrove CO2 efflux in the Florida coastal Everglades. *Agricultural and Forest Meteorology*, *213*, 273–282. https://doi.org/10.1016/j.agrformet.2014.12.012

Tully, K., Gedan, K., Epanchin-Niell, R., Strong, A., Bernhardt, E. S., Bendor, T., et al. (2019). The invisible flood: The chemistry, ecology, and social implications of coastal saltwater intrusion. *BioScience*, *69*(5), 368–378. https://doi.org/10.1093/biosci/biz027

Twilley, R. R., Rivera-Monroy, V. H., Chen, R., & Botero, L. (1999). Adapting an ecological mangrove model to simulate trajectories in restoration ecology. *Marine Pollution Bulletin*, *37*(8–12), 404–419. https://doi.org/10.1016/S0025-326X(99)00137-X

USDA-NRCS. (1996). Soil service of dade county area Florida.

Vaughn, D. R., Bianchi, T. S., Shields, M. R., Kenney, W. F., & Osborne, T. Z. (2020). Increased organic carbon burial in northern Florida mangrove-salt marsh transition zones. *Global Biogeochemical Cycles*, *34*(5), 1–21. https://doi.org/10.1029/2019GB006334

Vizza, C., West, W. E., Jones, S. E., Hart, J. A., & Lamberti, G. A. (2017). Regulators of coastal wetland methane production and responses to simulated global change. *Biogeosciences*, *14*(2), 431–446. https://doi.org/10.5194/bg-14-431-2017

Walcker, R., Gandois, L., Proisy, C., Corenblit, D., Mougin, É., Laplanche, C., et al. (2018). Control of "blue carbon" storage by mangrove ageing: Evidence from a 66-year chronosequence in French Guiana. *Global Change Biology*, *24*(6), 2325–2338. https://doi.org/10.1111/gcb.14100

Waldo, N. B., Hunt, B. K., Fadely, E. C., Moran, J. J., & Neumann, R. B. (2019). Plant root exudates increase methane emissions through direct and indirect pathways. *Biogeochemistry*, *145*(1–2), 213–234. https://doi.org/10.1007/s10533-019-00600-6

Whiting, G. J., & Chanton, J. P. (2001). Greenhouse carbon balance of wetlands: Methane emission versus carbon sequestration. *Tellus Series B Chemical and Physical Meteorology*, *53*(5), 521–528. https://doi.org/10.3402/tellusb.v53i5.16628

Wilson, B. J., Servais, S., Mazzei, V., Kominoski, J. S., Hu, M., Davis, S. E., et al. (2018). Salinity pulses interact with seasonal dry-down to increase ecosystem carbon loss in marshes of the Florida Everglades. *Ecological Applications*, *28*(8), 2092–2108. https://doi.org/10.1002/eap.1798

Wood, S. N. (2000). Modelling and smoothing parameter estimation with multiple quadratic penalties. *Journal of the Royal Statistical Society - Series B: Statistical Methodology*, *62*(2), 413–428. https://doi.org/10.1111/1467-9868.00240

Wood, S. N. (2006). *Generalized additive models*. Chapman and Hall/CRC. https://doi.org/10.1201/9781420010404

Wood, S. N. (2017). *Generalized additive models*. Chapman and Hall/CRC. https://doi.org/10.1201/9781315370279

Xiong, Y., Liao, B., & Wang, F. (2018). Mangrove vegetation enhances soil carbon storage primarily through in situ inputs rather than increasing allochthonous sediments. *Marine Pollution Bulletin*, *131*(682), 378–385. https://doi.org/10.1016/j.marpolbul.2018.04.043

Yu, Z., Staudhammer, C. L., Malone, S. L., Oberbauer, S. F., Zhao, J., Cherry, J. A., & Starr, G. (2022). Biophysical factors influence methane fluxes in subtropical freshwater wetlands using eddy covariance methods. *Ecosystems*, *26*(4), 706–723. https://doi.org/10.1007/s10021-022-00787-0

Zhang, C., Denka, S., Cooper, H., & Mishra, D. R. (2018). Quantification of sawgrass marsh aboveground biomass in the coastal Everglades using object-based ensemble analysis and Landsat data. *Remote Sensing of Environment*, *204*(May 2017), 366–379. https://doi.org/10.1016/j.rse.2017.10.018

Zhao, J., Malone, S. L., Staudhammer, C. L., Starr, G., Hartmann, H., & Oberbauer, S. F. (2021). Freshwater wetland plants respond nonlinearly to inundation over a sustained period. *American Journal of Botany*, *108*(10), 1917–1931. https://doi.org/10.1002/ajb2.1746

Zhao, J., Oberbauer, S. F., Olivas, P. C., Schedlbauer, J. L., May, J. L., Moser, J. G., et al. (2018). Contrasting photosynthetic responses of two dominant macrophyte species to seasonal inundation in an everglades freshwater prairie. *Wetlands*, *38*(5), 893–903. https://doi.org/10.1007/s13157-018-1038-1